

## ANALYSIS OF STABLE CRACK GROWTH OF A SEMI-ELLIPTICAL SURFACE CRACK BY NUMERICAL SIMULATION

G. Moussavi Zadeh

Bundesanstalt für Materialforschung und -prüfung (BAM), Berlin, Germany

### ABSTRACT

In the present paper, the canoeing effect during stable crack growth of a semi-elliptical surface crack in a side-grooved panel were investigated by means of a three-dimensional elastic-plastic finite element analysis. The influence of crack tip constraint and stress triaxiality on ductile crack resistance property were studied. It is shown that the tearing modulus  $T_{JR}$  increases proportional with decreasing stress triaxiality implying constraint dependent  $J_R$ -curves.

### 1. Introduction

From experimental observation it is well known that with the progress of stable crack growth of semi-elliptical surface cracks in panels or pressure vessels a "canoe" shaped crack front is formed. Based on the J integral concept the crack initiation and crack propagation in ductile materials are described by J resistance curves. The  $J_R$ -curves were found to be dependent on specimen geometry. Therefore, the transfer of these curves on surface flaws in components is no longer ensured. According to the HRR-theory, J-dominance and J-controlled crack growth require certain size conditions which were defined basically for compact specimens mit straight crack fronts. It is clear, that these requirements are violated by a Leak-Before-Break analysis requiring reliable crack resistance data up to 100% of the remaining ligament. Numerical investigations applying the J integral concept on stationary cracks in pressure vessels (1) show that the ductile crack growth observed in the experiment can not be described adequately by the single parameter concept of J controlled crack growth. The influence of the local stress triaxiality must be also considered (2).

The development of the canoe-effect in a semi-elliptical surface crack of a side-grooved panel (SCTsg) were analysed by a finite element simulation of stable crack growth. The numerical analysis were performed using local crack mouth opening displacement versus crack growth curves along the crack front obtained from experiments on panels by the multi specimen procedure. The simulation allows the determination of local  $J_R$ -curves which, correlated to the local multiaxiality of the stress state, were used to verify the constraint modified J concept. The results of the experimental investigation of side-grooved tension panels with surface flaws are presented in this conference by K. Wobst et al (3).

## 2. Constraint and stress triaxiality

The amount of plastic flow in a specimen or component is determined by the so-called constraint of the structure which reflects the specimen geometry and the type of loading (bending or tension). In three-dimensional configurations the constraint is due to effects directed parallel and perpendicular to the crack front. The first, named as "out-of-plane" constraint, is influenced by the thickness of the specimen and signified the approaching to the plane strain or plane stress condition. The second, referred to as "in-plane" constraint, is correlated to the ligament width. An increasing constraint causes a higher stress triaxiality (4,5). Because of its importance for the crack growth behaviour of a flawed structure it is needed to quantify constraint as well as stress triaxiality. A physically sound definition of the triaxiality of the stress state is given by the ratio  $h(r,\theta)$  of hydrostatic stress,  $\sigma_h$ , and von Mises equivalent stress,  $\sigma_e$ . The significance of this ratio for void growth in elastic-plastic materials is well-known, namely, for promoting void growth on the micromechanical level and thus causing damage in the process zone (6,7). The ratio  $h(r,\theta)$  is a local field quantity which varies not only with the crack front but also with the distance to the crack front,  $r$ , and ligament angle,  $\theta$ . In the present paper, the maximum value of this ratio,  $\chi$ , ahead of the crack tip is applied to characterize the dependency of the local  $J_R$ -curves on the triaxiality on the stress state (8). It is still a question under discussion how to quantify the crack tip constraint. Here, the tangential strain component,  $\epsilon_{tt}$ , and the normal strain component,  $\epsilon_{nn}$ , along the crack front are used for that purpose.

## 3. Numerical simulation of stable crack growth of a semi-elliptical surface crack

One-quarter of a SCTsg specimen was modelled for the FE analysis as shown in Figure 1 because of symmetry conditions. The FE model consists of 835 isoparametric quadratic brick elements with 4384 nodes. The regular small elements along the ligament are of a length of 0.2 mm. The FE calculations were performed with ADINA (9) using the incremental Prandtl-Reuss theory under materially non-linear only conditions. The numerical simulation of surface crack growth was modelled by using the node shifting and node release technique (10). The local crack growth  $\Delta a(\Phi)$  is controlled by the crack mouth opening displacement. The controlling CMOD( $\Phi$ ) resistance curves are plotted in Figure 2. Here, the different crack locations are designed by the angle  $\Phi$  as defined in Fig. 1. The J integral was evaluated with the virtual-crack extension-method of de Lorenzi (11) using a contour defined in the far field where J is still path-independent for extensive crack growth.

## 4. Results of the FE analysis

Figures 3 and 4 display the comparison of the numerical results with experimental data. The calculated load-CMOD-curve, shown in Figure 3, is in good agreement with the experimental records. Figure 4 compares the numerically simulated canoe shaped ductile crack growth with the experimentally obtained crack extension. The local crack growth,  $\Delta a(\Phi)$ , is measured perpendicular to the crack front. The maximum crack growth were calculated at  $\Phi \approx 60^\circ$ , whereas minimum crack growth were always obtained at  $\Phi = 90^\circ$  which is again in good agreement with experimental observations.

Figure 5 shows the variation of J integral along the crack front for several load steps. For low remote loading the J remains constant. At intermediate loads a local J maximum develops at  $\Phi = 60^\circ$  which is in correspondence with the local crack growth initiation. But, with increasing load a second maximum arises at the free surface ( $\Phi = 90^\circ$ ), i.e., the J

distribution along the crack front is no longer in agreement with the experimentally observed crack growth. The local crack resistance curves are plotted in Fig. 6 reflecting the different crack resistance behavior of a semi-elliptical surface crack by different slopes. It is shown, that the local crack resistance increases linearly with the crack extension. The highest slope of the  $J_R$ -curves were calculated at the free surface of the specimen, and their lowest slopes in the range of  $\Phi = 60^\circ$  to  $\Phi = 80^\circ$ . Alternatively to the global J integral concept a local CTOD concept is often used in non-linear fracture mechanics. A modified crack tip opening displacement,  $\delta_5$ , which is linearly related to the J integral, were introduced by Schwalbe and Hellmann (12). The local  $\delta_5(\Phi)$ -curves shown in Fig. 7 indicate the same local crack resistance against ductile tearing as it was predicted by the  $J_R(\Phi)$ -curves.

The side-grooving rises the constraint in a SCT specimen and effects the crack tip constraint along the crack front. The variation of the out-of-plane constraint,  $\epsilon_{tt}$ , and the in-plane constraint,  $\epsilon_{nn}$ , along the crack contour are plotted in Fig. 8. In contrast to normal strain,  $\epsilon_{nn}$ , the tangential strain,  $\epsilon_{tt}$ , increases at the deepest point of the crack ( $\Phi=0^\circ$ ) because of the higher constraint caused by the side-groovings. An opposite behaviour is shown at the free surface of the specimen. The highest crack tip constraint occurs near  $\Phi = 60^\circ$ , where  $\epsilon_{nn} \approx \epsilon_{tt}$ , and where the local crack growth initiation takes place.

Analogous to the treatment of the crack tip constraint the stress triaxiality has been divided into two parts, parallel to the crack front, expressed by  $\sigma_{tt} / (\sigma_{yy} + \sigma_{nn})$  as out-of-plane triaxiality, and perpendicular to it, with  $\sigma_{nn} / (\sigma_{yy} + \sigma_{tt})$  as in-plane triaxiality. Contrary to the out-of-plane triaxiality the in-plane triaxiality shows its minimum value at the panel center, see Figs. 9a,b. The stress state at the free surface approaches the plane stress state which in turn implies a decreasing stress triaxiality.

These quantities are used to describe how the geometrical effect of side-grooving influences the local crack tip constraint, the local stress triaxiality, and consequently the local crack resistance behaviour. But, it is shown, that they are not suitable to quantify the geometrical influence on  $J_R$ -curves significantly.

Figure 10 shows the  $\chi$  distribution in the ligament along the crack front for several load levels. The maximum values of  $\chi(\Phi)$  can be found in a range of  $\Phi = 60^\circ$  to  $\Phi = 70^\circ$  indicating the region of highest crack tip stress triaxiality. After crack growth initiation the  $\chi(\Phi)$  distribution remains almost constant. The variation of the stress triaxiality  $\chi(\Phi)$  along the crack front exposes the fact that the maximum of local crack growth coincides with the maximum of  $\chi(\Phi)$ . It is well known that lower constraint found in CCT specimens result in  $J_R$ -curves steeper than those obtained from CT specimens exhibiting a higher constraint. The slope of the  $J_R$ -curves,  $dJ/da$ , along the crack front obtained at a stable crack growth of  $\Delta a(\Phi) \approx 0.2$  mm, is correlated with the corresponding stress triaxiality  $\chi(\Phi)$  in Fig. 11. Both quantities, normalized with respect to their values at  $\Phi = 0^\circ$ , show an opposite behaviour in that the minimum of  $dJ_R/da$  is correlated with the maximum of  $\chi$ .

In contrast to  $\chi(\Phi)$  the distribution of  $J(\Phi)$  does not longer coincidence with the canoe shaped crack propagation. In order to ensure the transferability of resistance curves from test specimens to flawed structures the one parameter J concept must be correlated with  $\chi(\Phi)$ . To demonstrate the dependence of crack resistance curves on the  $\chi$ -parameter the normalized slope of  $J_R(\Phi)$ -curves, i.e. the tearing modulus  $T_{JR}$ , is plotted versus  $\chi(\Phi)$  at a stable crack growth of  $\Delta a(\Phi) \approx 0.2$  mm in Figure 12. Results obtained from side-grooved CT- and CCT-specimens are added. Independence of specimen geometries and type of loading is represented as a first approximation by a linear relation. With that simple assumption the resistance curves taken from test specimens can be used to describe quantitatively the ductile crack growth of components with surface flaws.

## Summary

The canoeing effect observed in experiments were attained by numerical simulation of stable crack growth of a semi-elliptical surface crack. The SCTsg specimen geometries affect the crack tip stress strain field and cause different crack tip constraint and stress triaxiality on the ligament along the crack front which influence the local crack resistance behaviour canoe shaped crack propagation. The  $\chi(\Phi)$ -parameter defined as the maximum ratio of hydrostatic stress,  $\sigma_h$ , over equivalent stress,  $\sigma_e$ , is apparently a significant measure to quantify the geometry effect on crack resistance tearing. The slope of the  $J_R$ -curve decreases with increasing  $\chi$ -parameter. By a simply assumption, namely a linear relationship between  $\chi$ -parameter and  $dJ_R/da$  the transferability of crack resistance curves of laboratory specimen on structures is assured.

## References

- [1] Brocks, B., et al.: Nucl. Engrg. and Design 135 (1992), pp. 151-160.
- [2] Aurich, D., Sommer, E.: Stell research 59 (1988), pp. 358-367.
- [3] Wobst, K., Hardtke, K.-D., Wossidlo, P.: paper G05/2.
- [4] Brocks, W., Schmitt, W.: EMAS (1990), pp. 1023-1032.
- [5] Clausmeyer, H. et al.: Mat.-wiss. u. Werkstoff. 20 (1989), pp. 101-117.
- [6] McClintock, F.A.: Trans. ASME, J. Appl. Mech. 35 (1968), pp. 363-371.
- [7] Rice, J.R., and Tracey, D.M.: J. Mech. Phys. Solids, Vol 17 (1969), pp. 201-217.
- [8] Brocks, W., Künecke, G.: Stell research 59 (1988), pp. 189-201.
- [9] Bathe, K.J.: Report AE 84-1, ADINA Engineering Inc., Watertown/MA.
- [10] Siegele, D. & Schmitt, W.: Computers & Structures 17 (1983), pp. 697-703.
- [11] Delorenzi, H. G.: J. of Fracture 19 (1982), pp. 183-193.
- [12] Schwalbe K.-H. , & Hellmann, D.: GKSS-Forschungszentrum Geesthacht., 1984, Bericht GKSS 84/E/37.

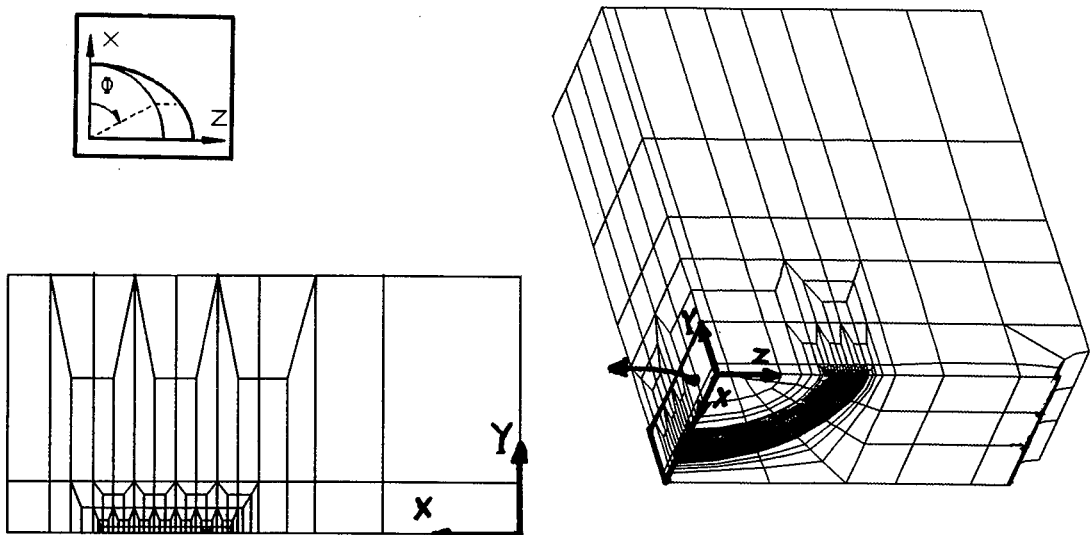


Figure 1: FE mesh of SCTsg specimen

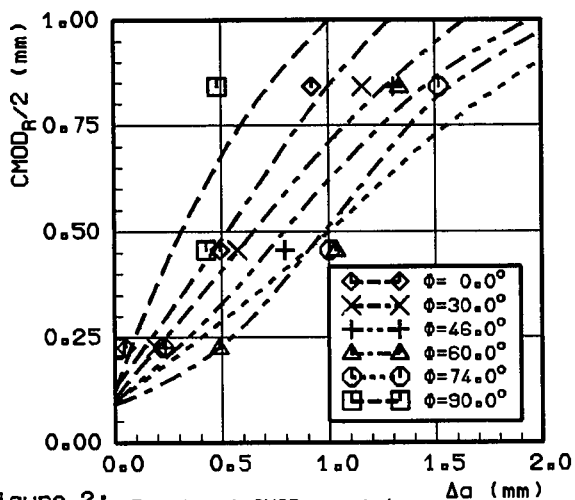


Figure 2: The local  $CMOD_R$  resistance curves of the surface crack

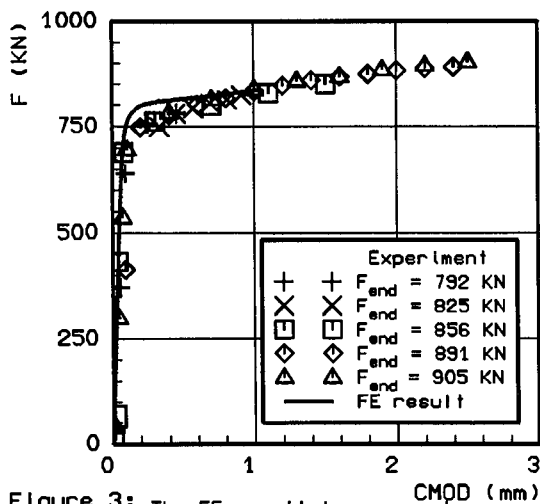


Figure 3: The FE result in comparison with experiment records

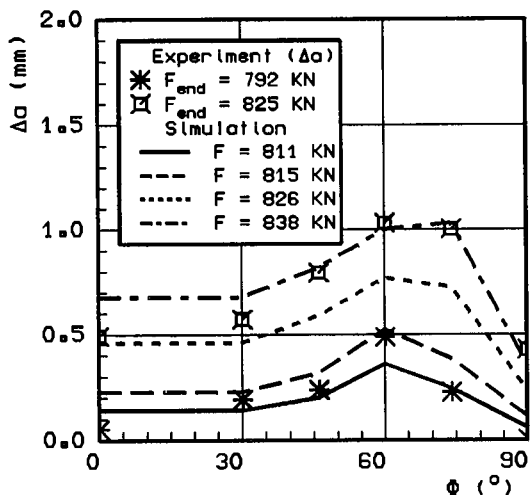


Figure 4: The cone shaped crack growth of the surface crack

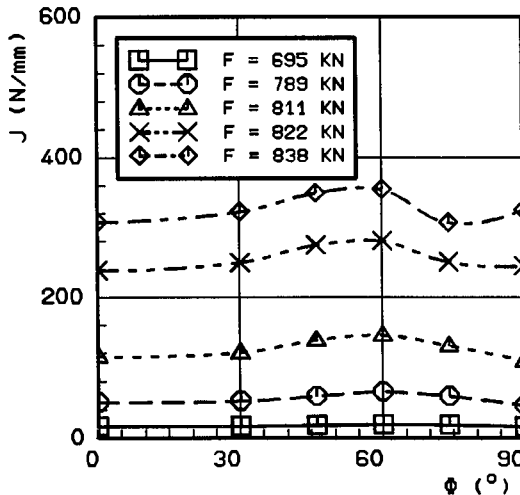


Figure 5: The J-variation along the crack front

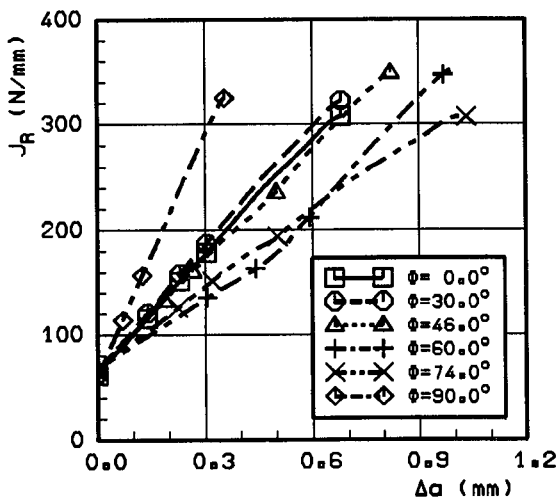


Figure 6: The local  $J_R$  resistance curves of the surface crack

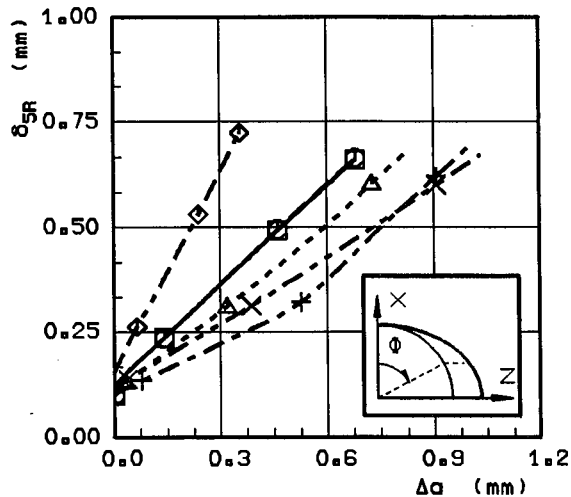


Figure 7: The local  $\delta_{5R}$  resistance curves of the surface crack

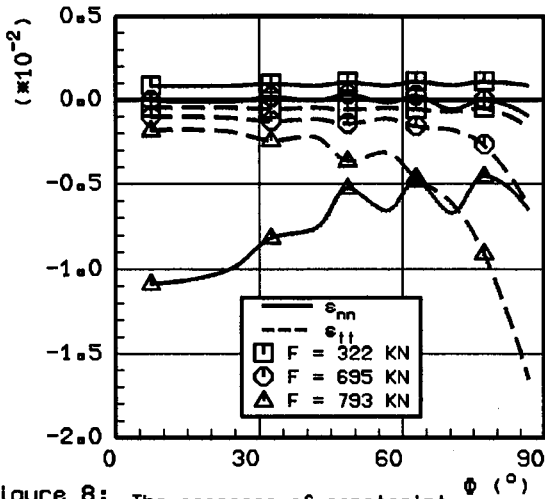


Figure 8: The progress of constraint in the ligament by  $r = 0.24$  mm

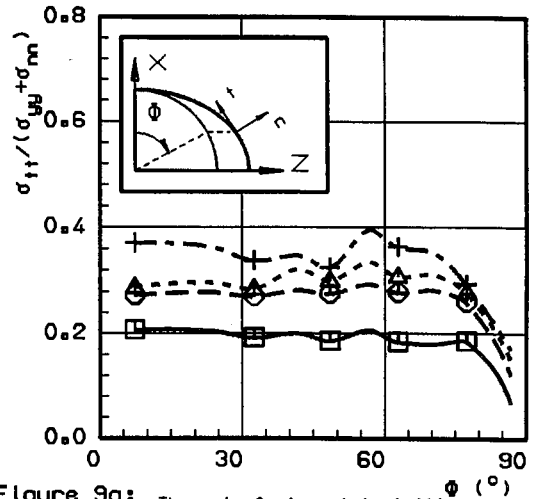


Figure 9a: The out-of-plane triaxiality in the ligament by  $r = 0.44$  mm

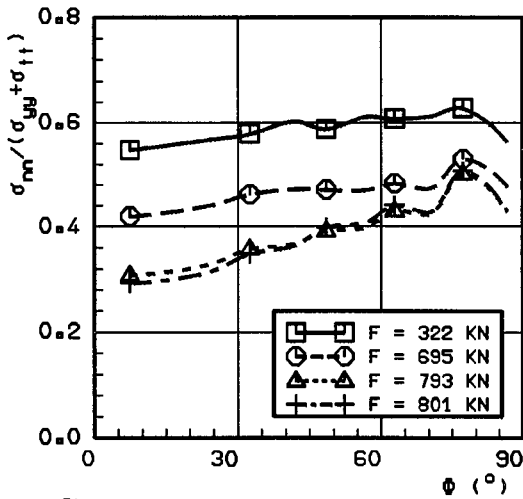


Figure 9b: The in-plane triaxiality in the ligament by  $r = 0.94$  mm

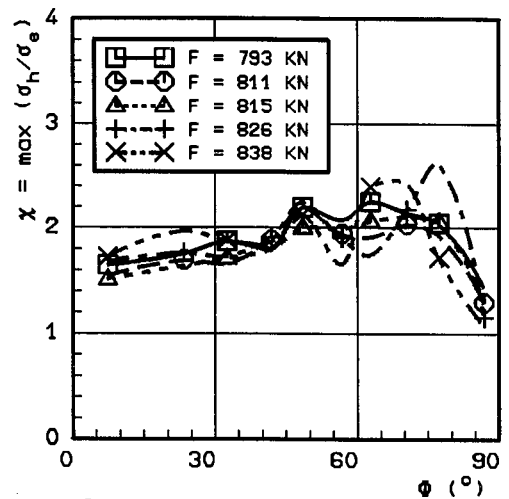


Figure 10: The maximum ratio of stress triaxiality in the ligament

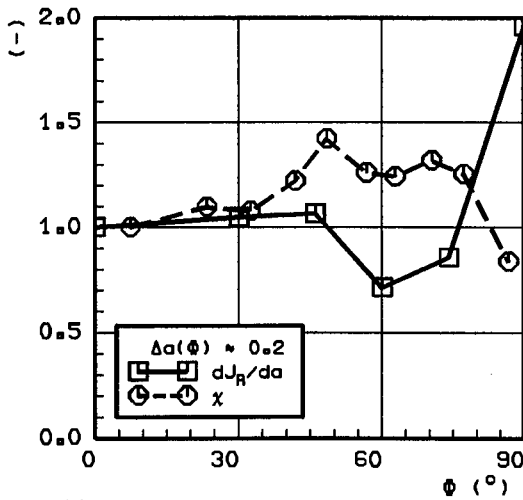


Figure 11: The influence of  $\chi$  on  $dJ_R/da$  (normalized)

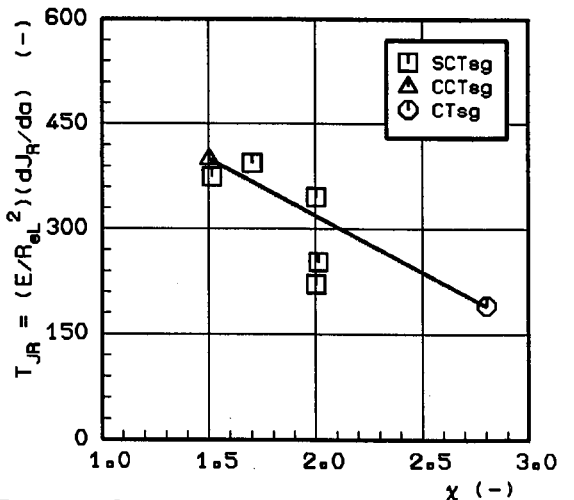


Figure 12: The relation between  $\chi$  and  $T_{JR}$  by  $\Delta a(\phi) \approx 0.2$  mm